Effect of the spin split-off band on optical absorption in p-type $Ga_{1-x}In_xAs_yP_{1-y}$ quantum-well infrared detectors

J. R. Hoff and M. Razeghi
Center for Quantum Devices, Northwestern University, Evanston, Illinois 60208

Gail J. Brown
Wright Patterson Air Force Base, Ohio 45433-7707

(Received 16 October 1995; revised manuscript received 6 May 1996)

Experimental investigations of p-type $Ga_{1-x}In_xAs_yP_{1-y}$ quantum-well intersubband photodetectors (QWIP's) led to the discovery of unique features in photoresponse spectra of these devices. In particular, the strong 2–5-μm photoresponse of these QWIP's was not anticipated based on previous experimental and theoretical results for p-type GaAs/Al_xGa_{1-x}As QWIP's. Our theoretical modeling of p-type QWIP's based on the $Ga_{1-x}In_xAs_yP_{1-y}$ system revealed that the intense short-wavelength photoresponse was due to a much stronger coupling to the spin-orbit split-off components in the continuum than occurs for GaAs/Al_xGa_{1-x}As QWIP's. Due to the strong influence of the spin split-off band, an eight-band Kane Hamiltonian was required to accurately model the measured photoresponse spectra. This theoretical model is first applied to a standard p-type GaAs/$Al_{0.3}Ga_{0.7}$As QWIP, and then to a series of GaAs/$Ga_{0.51}In_{0.49}P$, GaAs/$Ga_{0.62}In_{0.38}As_{0.22}P_{0.78}$, $Ga_{0.79}In_{0.21}As_{0.59}P_{0.41}/Ga_{0.51}In_{0.49}P$, and $Ga_{0.79}In_{0.21}As_{0.59}P_{0.41}/Ga_{0.62}In_{0.38}As_{0.22}P_{0.78}$ QWIP's. Through this analysis, the insignificance of spin split-off absorption in GaAs/Al_xGa_{1-x}As QWIP's is verified, as is the dual role of light-hole extended-state and spin split-off hole-extended-state absorption on the spectral shape of $Ga_{1-x}In_xAs_yP_{1-y}$ QWIP's. [S0163-1829(96)06840-3]

I. INTRODUCTION

Quantum-well intersubband photodetectors (QWIP's) are engineered optoelectronic devices which are designed from superlattices of relatively wide-band-gap III-V semiconductors. In a QWIP, the specific wavelengths of the response are not directly dependent on the band gaps of the constituent materials, but rather on the width and barrier height of the quantum wells in the superlattice. Therefore it is possible to design an infrared photodetector from materials that do not normally respond to infrared light—like GaAs and its related compounds. The potential benefits of quantum-well intersubband photodetectors are significant. First, by deliberate choice of well and barrier materials and well width, a designer is able to pick a particular wavelength range of interest. Second, by being able to use the mature growth and processing of GaAs and its related compounds, extremely high uniformities can be expected. In fact, the fabrication of large focal plane arrays on three inch wafers can readily be achieved.[1] For these two reasons, QWIP's have become the subject of intense research in the last few years.[1]

Most of the investigations thus far have been with n-type GaAs/Al_xGa_{1-x}As superlattices. Doping of the wells is required for photoresponse, and if the doping is n type then the conduction-band quantum well will be the source of infrared absorption. The results from these n-type devices have been good, but not good enough to unseat the industry standards. Therefore, work is being directed toward p-type QWIP's and toward alternative material systems in an effort to improve performance. The use of acceptor-doped GaAs quantum wells takes advantage of the inherent band mixing in the GaAs valence-band quantum well to overcome the normal incidence selection rule limitations of n-type QWIP's.[2] Moreover, the increased effective mass of the charge carriers in the valence-band quantum wells will result in a reduction in dark current and, consequently, a reduction in noise current.[1,3]

Recently, in a series of papers,[4,5] we demonstrated the superiority of aluminum-free, $Ga_{1-x}In_xAs_yP_{1-y}$-based p-type QWIP's. These devices demonstrated background-limited infrared photodetection (BLIP) up to sample temperatures in excess of 120 K for detectors with cutoff wavelengths between 3 and 7 μm. This high detector operating temperature, combined with the established benefits of replacing $Al_xGa_{1-x}As$ with $Ga_{1-x}In_xAs_yP_{1-y}$ materials in other optoelectronic devices,[6–9] suggest that acceptor-doped $Ga_{1-x}In_xAs_yP_{1-y}$ QWIP's have the potential to outperform donor-doped GaAs/Al_xGa_{1-x}As QWIP's. However, the spectral response of these aluminum-free QWIP's is unusually broad, covering a typical range of approximately 400 meV. To explain this behavior, it was necessary to model the band structure and the intersubband absorption processes in valence-band quantum wells.

Considerable work has been done on the analysis of intersubband absorption in semiconductor quantum wells. Chang and James[2] used a four-band envelope-function approximation, and showed that normal-incidence absorption is possible in valence-band quantum wells due to the mixing of the heavy-hole and light-hole valence bands away from the zone center. More recently, Szmulowicz,[10] and Szmulowicz and Brown[11] expanded the work of Chang and James by using an eight-band envelope-function approximation, and showed that the admixture of the spherically symmetric conduction band into the quantum-well states strongly enhanced normal incidence absorption. Furthermore, Szmulowicz[10] derived a general expression for the momentum matrix ele-

 © 1996 The American Physical Society

ments in the eight-band envelope-function approximation.

In their work with the eight-band envelope-function approximation, Szmulowicz and Brown utilized the fact that for a flatband condition in a symmetric quantum well, the wave function of the system is an eigenstate of parity. They determined the bulk band structure separately for the well and barrier of the quantum well, and then formed eigenstates of parity by linear combinations of the bulk bands. By using this technique, they were able to determine bound as well as continuum states. Moreover, they were able to do so without placing an arbitrary, nonphysical enclosure into their analysis. However, they have published information concerning only intersubband absorption for wavelengths longer than 5 μm, effectively ignoring the influence of the spin split-off band. This constraint is virtually inconsequential for the GaAs/$Al_{0.3}Ga_{0.7}As$ QWIP's that they were simulating and measuring. In $Al_{0.3}Ga_{0.7}As$, the spin split-off band is approximately 320 meV below the heavy- and light-hole energy level at the zone center.[12] However, in $Ga_{0.51}In_{0.49}P$ lattice matched to GaAs, the spin split-off band is only 94 meV below the heavy- and light-hole energy level at zone center, and thus its influence on continuum states is much stronger.

The results of our efforts to model the absorption mechanisms in p-type quantum wells will be presented in the following manner. Section II will briefly detail the theoretical and computational techniques used herein. Section III will present theoretical results of intersubband absorption in GaAs/$Al_xGa_{1-x}As$ superlattices for comparison with other published results, and as a reference by which the $Ga_{1-x}In_xAs_yP_{1-y}$ results can be gauged. Section IV will compare theoretical and experimental results for GaAs/$Ga_{0.51}In_{0.49}P$ superlattices, and present an explanation for their behavior. Section V will perform a similar analysis of quaternary-ternary, binary-quaternary, and fully quaternary-quaternary $Ga_{1-x}In_xAs_yP_{1-y}$ superlattices. It will be shown that the influence of the spin split-off band has a greater effect on these devices than it does on GaAs/$Al_xGa_{1-x}As$ devices, and that careful choice of $Ga_{1-x}In_xAs_yP_{1-y}$ materials in the well and barrier can either minimize or maximize the effect of the split-off band.

II. METHOD OF CALCULATION

As presented by Chang and James,[2] it is sufficient to demonstrate normal-incidence absorption in p-type quantum wells by using the four-band Luttinger-Kohn Hamiltonian, which is expressed across the two time-reversed components of both the heavy- and light-hole bands. However, Szmulowicz and Brown,[11] using the eight-band Kane Hamiltonian, were able to demonstrate an additional absorption mechanism due to the admixture of the spherically symmetric conduction band into the quantum-well states. For $Ga_{1-x}In_xAs_yP_{1-y}$ superlattices, there is even greater reason to use the eight-band model. The spin split-off band in $Ga_{1-x}In_xAs_yP_{1-y}$ compositions lattice matched to GaAs plays an important role in the band structure and optical matrix of a quantum well for two principal reasons.

First, the valence-band quantum wells of the $Ga_{1-x}In_xAs_yP_{1-y}$ system are, in general, deeper than those of the $Al_xGa_{1-x}As$ system. In spite of the fact that the spin split-off energy of GaAs is relatively large (340 meV), the $Ga_{1-x}In_xAs_yP_{1-y}$ valence-band offsets can be comparable in energy, especially for compounds close to $Ga_{0.51}In_{0.49}P$. This forces the bottom of the split-off quantum well—i.e., the quantum well formed by the split-off bands—to be closer to the top of the standard quantum well—i.e., the quantum well formed by the light- and heavy-hole bands. One side note appropriate at this time is that because these are valence-band quantum wells, the energies are negative. The authors will attempt to maintain the convention of negative energies in most cases. However, it is most convenient to speak of the highest negative energies inside a valence-band quantum well as the top of the quantum well. Consequently, the lowest negative energies inside a valence-band quantum well are the bottom of the quantum well. Using this convention, a list of the quantum-well edges in order of decreasing energy (or increasing negative energy) of a typical GaAs/$Al_{0.3}Ga_{0.7}As$ quantum well would be, first, the bottom of the standard quantum well; second, the top of the standard quantum well; third, the bottom of the split-off quantum well; and, fourth, the top of the split-off quantum well.

The second reason that an eight-band Hamiltonian is necessary is that the spin split-off energy of barrier compounds is typically small especially for those compounds close in composition to $Ga_{0.51}In_{0.49}P$. Thus the perturbation caused by the split-off quantum well cannot be ignored. There is a smooth, compositionally dependent transition of $Ga_{1-x}In_xAs_yP_{1-y}$ spin split-off energies from GaAs (340 meV) to $Ga_{0.51}In_{0.49}P$ (94 meV). Therefore, the closer that a compound is to $Ga_{0.51}In_{0.49}P$, the closer the spin split-off band is to the heavy-hole–light-hole zone-center valence-band maximum. This means that the closer a barrier compound is to $Ga_{0.51}In_{0.49}P$, the closer the top of the split-off quantum well is to the top of the standard quantum well. The closer a well compound is to $Ga_{0.51}In_{0.49}P$, the closer the bottom of the split-off quantum well is to the bottom of the standard quantum well.

The Kane Hamiltonian expressed across the $|X\uparrow\rangle$, $|Y\uparrow\rangle$, $|Z\uparrow\rangle$, and $|S\uparrow\rangle$ zone-centered Bloch functions and their time-reversed conjugates $|X\downarrow\rangle$, $|Y\downarrow\rangle$, $|Z\downarrow\rangle$, and $|S\downarrow\rangle$ was used as the starting point[13] of this analysis. However, this Hamiltonian is by definition a bulk Hamiltonian, and an additional computational technique is necessary to make it appropriate for use with quantum wells. The eigenfunction expansion method was chosen for the evaluation.[14] By this method, the eigenfunctions of the Kane Hamiltonian are expanded as a discrete Fourier transform across a set of functions periodic on the superlattice period. This places a periodic boundary condition on the analysis, but, in any QWIP, the photodetector is constructed of periodic superlattices making a periodic boundary condition well suited to the analysis. Unfortunately, this periodic boundary condition does force an artificial quantization on the analysis. This artificial quantization will not be noticeable for bound states in the quantum well, but it will be apparent in the continuum above the barriers, which, rather than being a perfect continuum will resemble a huge set of discrete states separated by a few meV. An infinite number of expansions would result in a perfect replication of the continuum, but this is impossible for a computer. Nevertheless, appropriate selection of the number of expansions and the width of the superlattice period will minimize

the effect of this artificial quantization.

A general form for the momentum matrix in the 8×8 envelope-function approximation has been derived by Szmulowicz for eigenfunctions in real space. This equation takes into account all interband and intraband optical transitions possible in a semiconductor quantum well. From Ref. 10,

$$M_{f,i}=\frac{\hbar}{m_0}\,\mathbf{e}\cdot\mathbf{P}_{f,i}=\left(\frac{\hbar^2}{m_0}\right)\mathbf{e}\cdot\sum_{i,f}\left\{\int dz\; F_f(Nk_\parallel,z)^*\times P_{i,f}(k_\parallel,z)F_i(Mk_\parallel,z)+\tfrac{1}{2}\int dz\times\left[-i\,\frac{d}{dz}\,F_f(Nk_\parallel,z)\right]^* Q_{i,f}(k_\parallel,z)F_i(Mk_\parallel,z)+\tfrac{1}{2}\int dz\; F_f(Nk_\parallel,z)^*Q_{i,f}(k_\parallel,z)\times\left[-i\,\frac{d}{dz}\,F_i(Nk_\parallel,z)\right]\right\}, \tag{1}$$

where $F_{i,f}$ are the real-space eigenfunctions of the initial and final states, and P and Q are the interaction matrices which are determined by the first and second derivatives of the Kane Hamiltonian. Unfortunately, this equation is not appropriate for the eigenfunction expansion method, since the eigenfunction expansion method converts the eigenfunctions into reciprocal space. Therefore, it was necessary to rederive Eq. (1) into a form more suitable to the computational technique. The result of the derivation is

$$\frac{\hbar}{m_0}\,\mathbf{e}\cdot\mathbf{P}=\sum_{i,f}\sum_{j,j'}F^*_{f,j}F_{i,j'}\left\{\left[\left(P_{i,f,0}+\left(\frac{2\pi j}{Z}\right)Q_{i,f,0}\right)+\sum_{n=2}^{N}\left[(P_{i,f,n}-P_{i,f,0})+\left(\left(\frac{2\pi j}{Z}\right)\times(Q_{i,f,n}-Q_{i,f,0})\right)\right]\left(\frac{z_{r,n}-z_{l,n}}{Z}\right)\right]\times\delta_{j,j'}+\frac{1}{2\pi i(j-j')}\sum_{n=2}^{N}\left[(P_{i,f,n}-P_{i,f,0})+\left(\left(\frac{\pi(j+j')}{Z}\right)(Q_{i,f,n}-Q_{i,f,0})\right)\right]\times(e^{2\pi i(j-j')(z_{r,n}/Z)}-e^{2\pi i(j-j')(z_{l,n}/Z)})\right\}, \tag{2}$$

where j and j' are integers which come from the discrete Fourier expansion of the initial and final states; $F_{fj'}$, and F_{ij}, are the reciprocal space eigenvector elements; $z_{r,n}$ and $z_{l,n}$ represent the position of the right and left interfaces of layer n in the superlattice period, and Z represents the width of superlattice period. Finally, $P_{i,f,n}$ and $Q_{i,f,n}$ are the elements of the interaction matrices for layer n determined from the Hamiltonian. The elements of the P and Q matrices are considered to be stepwise continuous across each period of the superlattice. For example, in a simple heterostructure,

TABLE I. Material parameters used in the simulations.

	GaAs	InAs	InP	GaP	GaInP
E_g	1.51 eV[a]				2.0 eV[a]
Δ	340 meV[b]	380 meV[b]	108 meV[b]	80 meV[c]	94 meV[d]
γ_1	6.85[b]	19.67[b]	6.28[b]	4.20[c]	5.2192[d]
γ_2	2.10[b]	8.37[b]	2.08[b]	0.98[c]	1.519[d]
γ_3	2.90[b]	9.29[b]	2.76[b]	1.66[c]	2.199[d]
m_e^*	0.067[b]				0.1175[e]

[a]Verified experimentally.
[b]D. Gershoni, C. H. Henry, and G. A. Baraff, IEEE J. Quantum Electron. **29**, 2433 (1993).
[c]Reference 15.
[d]Linear interpolation from binaries.
[e]F. Omnes and M. Razeghi, Appl. Phys. Lett. **59**, 1034 (1991), and references therein.

$$P_{i,f}(z)=P_{i,f_0}+[P_{i,f_1}-P_{i,f_0}]\Theta(z-z_0), \tag{3}$$

where $\Theta(z-z_0)$ is a step function. The variable z_0 is the position of the heterostructure interface, and $\Theta(z-z_0)$ is equal to zero on the left side of z_0 (in the first material) and equal to 1 on the right side of z_0 (in the second material). Equation (3) shows that $P_{i,f}(z)$ is a constant on either side of z_0, and that it changes instantaneously at the interface z_0. In a superlattice, the equation describing the spatial dependence of $P_{i,f}$ is more complicated, but, in principle, it is the same as Eq. (3). The elements of the interaction matrices are viewed as constants in each well or barrier region, and those constants are considered to change instantaneously at the interface between any two layers.

The absorption coefficient was determined from the optical matrix by the equation

$$\alpha(\omega)=\frac{q^2}{ncm_0\omega L_W}\sum_{i,f}\int dk_\parallel 2\pi k_\parallel|\mathbf{P}|^2 f_0(E_f,E_i)\times\frac{\Gamma}{(E_f-E_i-\hbar\omega)^2-\Gamma^2} \tag{4}$$

where L_w is the width of the well, n is the refractive index, c is the speed of light, m_0 is the free-electron mass, f_0 is the Fermi function, and Γ is a broadening factor chosen to be 7 meV.[2] The absorption coefficient was evaluated by assuming a cylindrical symmetry in $k_\parallel$ space, and evaluating only along the $\langle 11\rangle$ direction. This assumption is inconsequential to the analysis. The use of a single artificial broadening factor for bound-to-continuum transitions like these, when coupled with the periodic boundary conditions of the eigenfunction expansion method, breaks the absorption coefficient into a number of sharp peaks at shorter wavelengths. This minor inconvenience could be overcome by adjusting the broadening factor or the superlattice period. However, this was not done in the present analysis.

Table I lists the material parameters used in the simula-

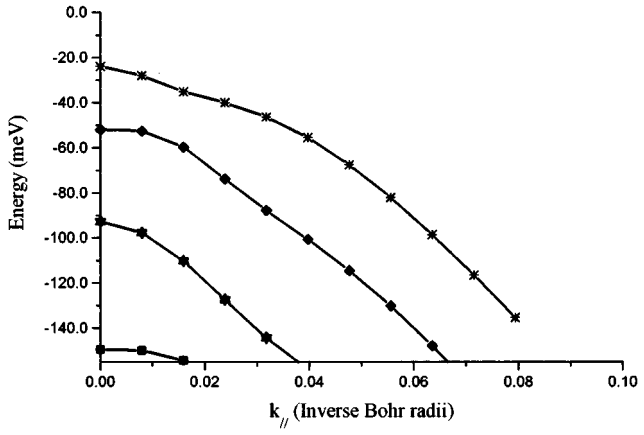

FIG. 1. The bound states of the standard quantum well (light-hole–heavy-hole quantum well) for a GaAs/$Al_{0.3}Ga_{0.7}As$ QWIP with 50-Å-wide wells and 500-Å-wide barriers. The results are identical to those published for the same quantum well in Ref. 10. The x axis is in inverse Bohr radii to facilitate comparison (the Bohr radius is 0.529 177 Å).

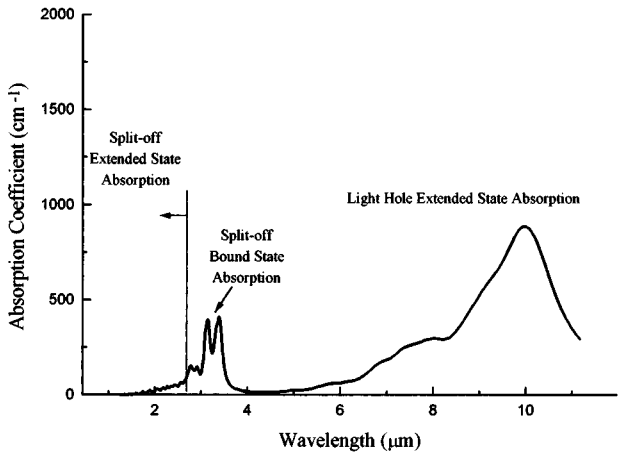

FIG. 2. The calculated absorption coefficient for the 50 Å/500 Å GaAs/$Al_{0.3}Ga_{0.7}As$ QWIP including the influence of the split-off band. The knee at approximately 8.5 μm is due to the artificial broadening. The vertical line indicates the onset of split-off extended-state absorption. Split-off absorption between 4 and 2.75 μm is bound, and does not contribute to the photoresponse.

tions. Bulk band gaps were determined by experiment using photoluminescence and photovoltaic spectroscopy. Spin-orbit splitting parameters and Luttinger parameters were taken from literature[15,7] for the binaries GaAs, GaP, InAs, and InP. For ternary and quaternary compounds, the same parameters were determined by linear interpolation from the binaries. The conduction-band effective mass of quaternary compounds was determined by linear interpolation between GaAs and $Ga_{0.51}In_{0.49}P$.

III. GaAs/$Al_{0.3}Ga_{0.7}As$ QWIP's

The photoresponse of p-type GaAs/$Al_xGa_{1-x}As$ QWIP's has been reported on a few occasions.[1,11,12] The most in-depth analysis, including both experimental results and theoretical work, was done by Szmulowicz and Brown.[11,12] Their analysis included the band structure and absorption coefficient of a QWIP with 50-Å-wide wells of GaAs, and 500-Å-wide barriers of $Al_{0.3}Ga_{0.7}As$. Using the material parameters given by Brown and Szmulowicz,[12] an identical analysis was performed by the eigenfunction expansion method.

Figure 1 shows the resultant band structure in the ⟨11⟩ direction. To facilitate comparison, the $k_{\|}$ axis in Fig. 1 is given in inverse Bohr radii as was done in Ref. 12. Nine expansion functions were all that was necessary to reach convergence for the bound states. However, since in the eigenfunction expansion method higher-energy states take more expansions to settle into their final value, 25 expansions were eventually used to ensure proper determination of the continuum bands.

Figure 2 shows the absorption coefficient for the same superlattice in the ⟨11⟩ direction. Again, the results are very similar to those of Refs. 11 and 12. However, the shortest wavelength displayed in Refs. 11 and 12 was approximately 5 μm. This is not high enough in energy to see the influence of the spin split-off band. Figure 3 shows the zone-centered quantum-well energy levels of the GaAs/$Al_{0.3}Ga_{0.7}As$ QWIP in question. The influence of the spin split-off quantum well will not be felt for nearly 190 meV below the top of the $Al_{0.3}Ga_{0.7}As$ barrier (i.e., higher negative energy). This places the split-off absorption at wavelengths shorter than approximately 4 μm (-125 meV$+-190$ meV$=-315$ meV). Our analysis extends below 4 μm, and includes the influence of the spin split-off band.

It would appear from first glance at Fig. 2 that the influence of the split-off band should have been observed experimentally, since it would seem that such an absorption would contribute significantly to photoresponse. However, an analysis of the decomposition of the eigenstates into their heavy-hole, light-hole, and split-off components shows that eigenstates with greater negative energies than -315 meV consist mainly of split-off states. Unfortunately, due to the large spin orbit splitting energy in the $Al_{0.3}Ga_{0.7}As$ barrier ($\sim$320 meV), all states with negative energies smaller than -125 meV$+-320$ meV$=-445$ meV are bound inside the split-off quantum well. Since these states are confined, charge carriers excited to these states cannot contribute significantly to the measured photoresponse signal. This leaves only the unconfined split-off extended states, with negative energies greater than the top of the split-off quantum well, to contribute to photoresponse, and those states begin around 2.75 μm. It is obvious from Fig. 2 that, for wavelengths shorter than 2.75 μm, the optical absorption resulting from the influence of the spin split-off band is virtually inconsequential when compared to optical absorption at longer wavelengths which results from light-hole extended states.

In conclusion, it can be seen that the influence of the spin split-off band has no effect on the optical absorption of p-type GaAs/$Al_xGa_{1-x}As$ QWIP's at the longer wavelengths for which these detectors were designed. Moreover, due to the depth of the split-off quantum well, there will be no significant contribution to photoresponse at shorter wavelengths. Therefore, in agreement with previous research, the split-off band does not play a major role in the photoresponse of p-type GaAs/$Al_{0.3}Ga_{0.7}As$ QWIP's.[11,12]

IV. GaAs/$Ga_{1-x}In_xP$ QWIP's

A. Experimental results

Three multiquantum-well infrared detector structures were grown on semi-insulating GaAs substrates by low-

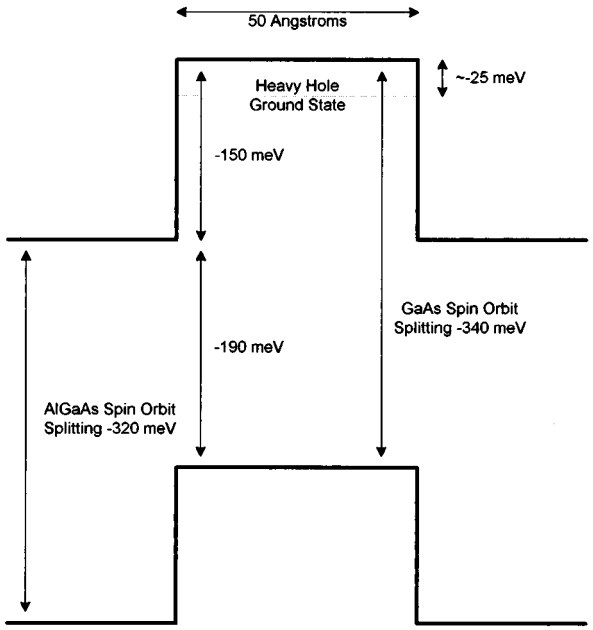

FIG. 3. A graphical depiction of the standard quantum well (formed by the bulk light- and heavy-hole bands) and the split-off quantum well (formed by the bulk split-off bands) for a $GaAs/Al_{0.3}Ga_{0.7}As$ quantum well. Of importance is, first, the separation between the bottom of the split-off quantum well from the top of the standard quantum well and second, the depth of the split-off quantum well. Both contribute to the reduction of split-off absorption in p-type $GaAs/Al_{0.3}Ga_{0.7}As$ QWIP's.

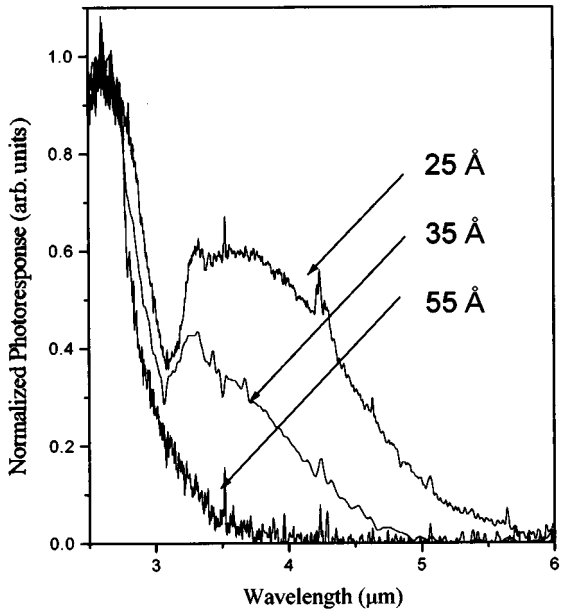

FIG. 4. The spectral response of the three different $GaAs/Ga_{0.51}In_{0.49}P$ QWIP samples under a bias of approximately 10 V. Note first the separation between the cutoff wavelength and the peak wavelength. Note also the change in shape with decreasing well width that occurs for the longer wavelengths.

pressure metal-organic chemical-vapor deposition. Each structure contains 50 GaAs quantum wells separated by 280-Å-wide $Ga_{0.51}In_{0.49}P$ barriers. This superlattice is cladded between thick GaAs layers used for top (0.5 μm thick) and bottom (1 μm thick) contact. All GaAs layers were doped with zinc to a net acceptor concentration of $2–3\times10^{18}$ cm^{-3}. Different GaAs well widths (25, 35, and 55 Å) were used for the three different structures. Structural parameters were verified by x-ray diffraction and simulation. The individual detector mesas (400×400 μm^2) were fabricated using photolithography and wet chemical etching, and 100×100-μm^2 square Au/AuZn electrodes were evaporated and alloyed on the contact layers. Small arrays of these detector mesas were mounted on copper heat sinks, and front illuminated inside a liquid-nitrogen cryostat.

The normalized spectral responses for all three samples, at a bias of approximately 10 V, are shown in Fig. 4. There are a number of noteworthy features in these spectra. First, the cutoff wavelength increases with decreasing well width, as expected from theory. As the ground-state energy is pushed to higher negative energies in the well with decreasing well width, the energy required to escape the well decreases. In order to simulate this shift in the wavelength, the cutoff wavelength is defined as the wavelength corresponding to the energy difference between the heavy-hole ground state at the zone center and the top of the barrier. Using an effective-band-offset ratio ($\Delta Ec/\Delta Eg$) of 30%, this simulation was performed using both a simple Kronig-Penney model[16] and the more advanced Kane model.[13] Figure 5 shows the results of these simulations and compares them with the experimentally determined cutoff wavelength for near-zero-bias conditions. The agreement is good. Also of note in Fig. 4 is the broad spectral response and the apparent peak at short wavelength. These features are unique to this type of QWIP. QWIP's based on other material systems such as $GaAs/Al_xGa_{1-x}As$ typically display a narrow spectral response, especially n-type QWIP's,[1] but even in p-type $GaAs/Al_xGa_{1-x}As$ QWIP's, the peak wavelength is usually within approximately 30–50 meV of the cutoff wavelength.[12]

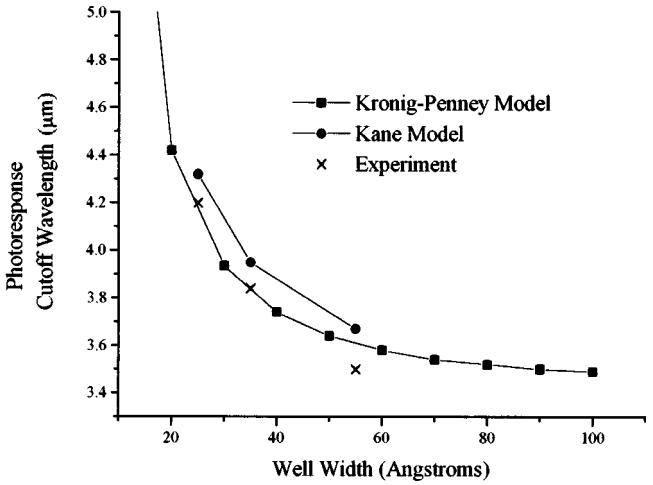

FIG. 5. A plot of the theoretically predicted and experimentally measured cutoff wavelengths for the different $GaAs/Ga_{0.51}In_{0.49}P$ QWIP's. Both the Kronig-Penney model and the Kane model were used for the theory. The agreement is good for a $\Delta Ec/\Delta Eg$ ratio of 30%.

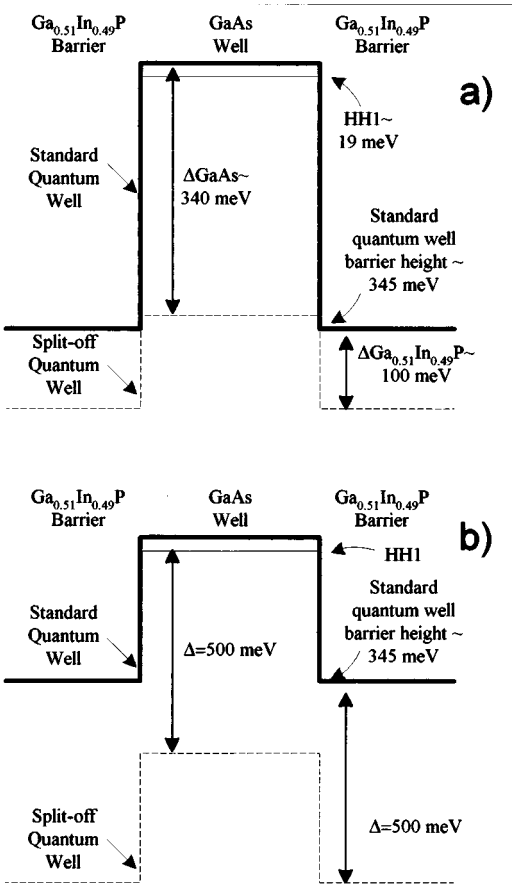

FIG. 6. A graphical depiction of the standard quantum well (formed by the bulk light- and heavy-hole bands) and the split-off quantum well (formed by the bulk split-off bands) for the two different simulations of the $GaAs/Ga_{0.51}In_{0.49}P$ QWIP's. (a) is the true simulation, and represents what is actually present in these devices. (b) is accurate to reality in all but the spin-orbit splitting energy, which is increased to remove the effect of the split-off band.

B. Sample 1: The 55-Å-wide well

Two different simulations were performed for each of the $GaAs/Ga_{0.51}In_{0.49}P$ samples. The first simulation was true to reality and will be referred to as the true simulation. In other words, the Luttinger parameters, energy gaps, and spin-orbit splitting parameters were all accurate to experimental values and to literature. In the second simulation, the same accuracy was used for all parameters except for the spin-orbit splitting parameters, which were increased to 500 meV for both the well and the barrier. The purpose of this second simulation was to remove the influence of the spin-orbit band, and to gain a greater insight into the physical mechanisms involved in optical absorption. Figure 6 shows schematics of the quantum wells used in the two simulations.

Figure 7 shows all of the bound states inside the standard quantum well for both simulations of a $GaAs/Ga_{0.51}In_{0.49}P$ QWIP with 55-Å-wide wells. The results on the right-hand side of Fig. 7 are for the true simulation. Also shown in this figure are the first of the continuum states below the barrier. Note that this continuum state is not parabolic in the true simulation, but rather displays some anticrossing behavior typical of a bound state. This behavior results from the presence of the spin split-off quantum well, which is located at

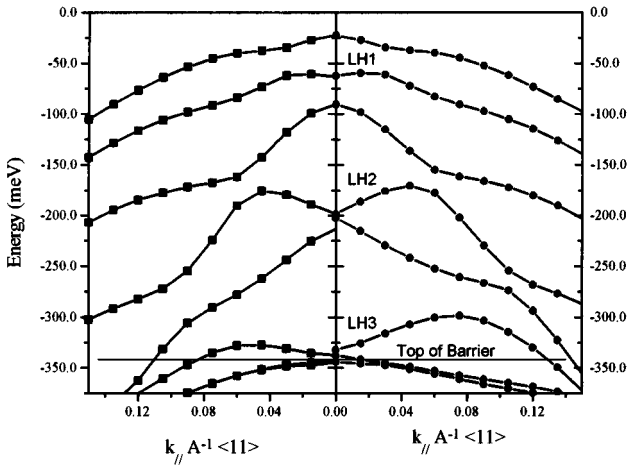

FIG. 7. The band structure of the $GaAs/Ga_{0.51}In_{0.49}P$ QWIP with 55-Å-wide wells using both the true simulation (right-hand side) and the second simulation with the split-off band removed (left-hand side). The bound light-hole bands are listed LH1, LH2, and LH3. The energy level of the top of the quantum-well barrier is indicated. The continuum states are those states whose zone-center ($k_{\|}=0$) energy is below the top of the barrier. Note that the continuum states on the left are more parabolic, and show no anticrossing behavior.

the top of the standard quantum well and imparts a boundlike nature to the split-off components of these states. In the case of the second simulation shown on the left of Fig. 7, the more tightly bound quantum-well states like the heavy-hole ground state are unaffected by the removal of the split-off band, but the higher-energy states near the top of the standard quantum well are changed, especially away from the zone center. Moreover, the continuum states below the standard quantum well are much more parabolic in the second simulation, indicating that these states are more like the continuum of an ideal quantum well.

Figure 8 shows the absorption coefficient as a function of wavelength for both simulations. The graph on the top (a) is for the true simulation. There are a number of important features consistent between the experimental photoresponse and the calculated absorption spectra. The most basic of the consistencies is the cutoff wavelength, which was described previously. In addition, the simulation reveals significant absorption over a broad spectral range which is consistent with the observed photoresponse. What differs, however, is the presence of significant absorption at 3.5 μm which is not reflected in the photoresponse. This can be explained simply as a bound state inside the split-off quantum well. The heavy-hole ground-state energy is located 22.6 meV below the bulk valence-band maximum at zone center. Therefore, with a barrier height of roughly 345 meV, the minimum energy required for a hole to be excited into the continuum is about 322 meV or 3.87 μm. Similarly, the onset of spin split-off extended states is related to the energy difference between the heavy-hole ground state and the top of the split-off quantum well. Since the spin-orbit splitting energy of the $Ga_{0.51}In_{0.49}P$ barrier is approximately 94 meV, the onset occurs at 416 meV or 2.98 μm. Therefore, the peak at 3.5 μm must be inside the spin split-off quantum well. Further confirmation comes from a weight decomposition of the eigenstates into their heavy-hole, light-hole, and split-off compo-

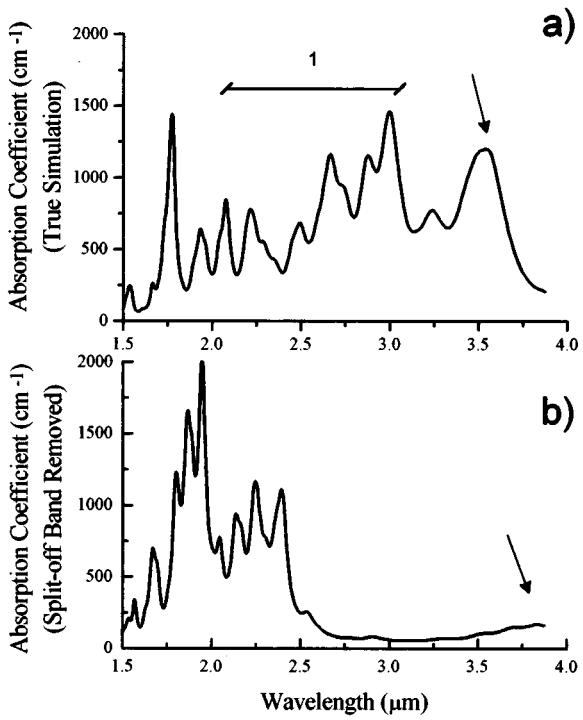

FIG. 8. The calculated absorption coefficient for the $GaAs/Ga_{0.51}In_{0.49}P$ QWIP with a 55-Å-wide well. (a) The true simulation. The arrow indicates the bound split-off state that cannot contribute to the photoresponse. The number 1 indicates the range of split-off extended-state absorption. (b) The second simulation removing the split-off band. The arrow indicates the small light-hole extended-state absorption at long wavelengths.

nents. This decomposition reveals that the states around 3.5 μm are dominated by split-off components. Due to the relatively heavy mass of the holes, the likelihood of tunneling out of the split-off quantum well is small. So, in spite of the significant absorption, at 3.5 μm there will be no contribution to photoresponse. Figure 8(a) also shows that the highest absorption occurs for energies below 3.0 μm. This wavelength is consistent with the first of the unbound split-off extended states.

As an additional test of the influence of the spin split-off quantum well on the bound-to-continuum photoresponse, a second simulation was run using an artificial spin-splitting energy of 500 meV for both well and barrier materials. The results of the second simulation are shown in Fig. 8(b). In this case, the split-off absorption has been shifted to wavelengths shorter than 2.5 μm, which is the wavelength consistent with the bottom of the ''new'' split-off band. The absorption that remains in the photoresponse range of the QWIP (see Fig. 4) can be attributed to transitions to light-hole extended states in the continuum of the standard quantum well. Looking at the band structures in Fig. 7, it is readily apparent that the fourth light-hole state is the first light-hole extended state. The coupling between the heavy-hole ground state and the fourth light-hole state is minimal. Therefore, there is little absorption between 2.5 and 3.87 μm. This is significant because transitions to light-hole extended states could have contributed to photoresponse, even though these states are within the energy range of the split-off quantum well.

In conclusion, it can be seen from the two simulations that the broad spectral response is due to the influence of the split-off band. In this case of the $GaAs/Ga_{0.51}In_{0.49}P$ QWIP with 55-Å-wide wells, there is significant absorption between the cutoff at 3.87 μm down to approximately 1.5–2 μm. However, weight decomposition analysis showed that the significant absorption contribution at wavelengths longer than 2.98 μm was due to bound split-off states. The second simulation showed that the light-hole extended state absorption that remained after the split-off band was removed was insignificant. Thus significant photoresponse can only occur for wavelengths shorter than 2.98 μm, which correspond to transitions between the heavy-hole ground state and split-off extended states. This analysis is very consistent with the observed photoresponse spectrum, which shows a cutoff wavelength around 3.5 μm, very little photoresponse between 3.5 and approximately 2.9 μm, and then a sharp increase in photoresponse which appears to peak around 2.5 μm.

C. Sample 2: The 25-Å-wide well

Looking again at Fig. 4, it is obvious that the short-wavelength features of the three photoresponse spectra are very similar. This is to be expected since they are all $GaAs/Ga_{0.51}In_{0.49}P$ superlattices and, therefore, are all subject to the strong influence of the close split-off band. In particular, peak photoresponse should depend strongly upon heavy-hole ground state to split-off extended-state transitions. However, as the width of the well is narrowed in Fig. 4, not only does the cutoff wavelength shift, but also the magnitude of the photoresponse at longer wavelengths increases significantly. Further analysis is needed to explain this change in the photoresponse cross section.

A band structure analysis of the 25-Å-wide well indicates that the heavy-hole ground-state energy is 73.7 meV below the bulk zone-center valence-band maximum. This means that, for the approximately 345-meV valence-band quantum-well barrier height, the cutoff wavelength is about 4.6 μm (or 271 meV). Similarly, the onset energy for transitions to the split-off extended states now occurs at 365 meV or approximately 3.4 μm. Therefore, the peak in the photoresponse which occurs at approximately 3.75 μm (Fig. 4) is clearly in the same energy range as the split-off quantum well. For reasons described in Sec. IV B, this peak response cannot be attributed to the split-off absorption. There must be other transitions to consider in the case of the 25-Å well. The band-structure analysis shows that the second light-hole state was pushed into the continuum of the standard well, and is in the energy range of the split-off quantum well. In addition, there is only one split-off bound state, located near the top of the split-off quantum well.

To separate the effects of these two possible transitions, simulations with and without a nearby split-off band were carried out, as was described for the 55-A QWIP. Figure 9 shows the absorption coefficient calculated for a $GaAs/Ga_{0.51}In_{0.49}P$ QWIP with 25-Å-wide wells using both simulation techniques. Once again, removing the split-off band reveals the presence of light-hole extended-state absorption. This time, however, since the second light-hole state is now in the continuum of the standard quantum well, the absorption at longer wavelengths is significant. Therefore, Fig. 9 reveals that the spectral shape of the 25-Å QWIP

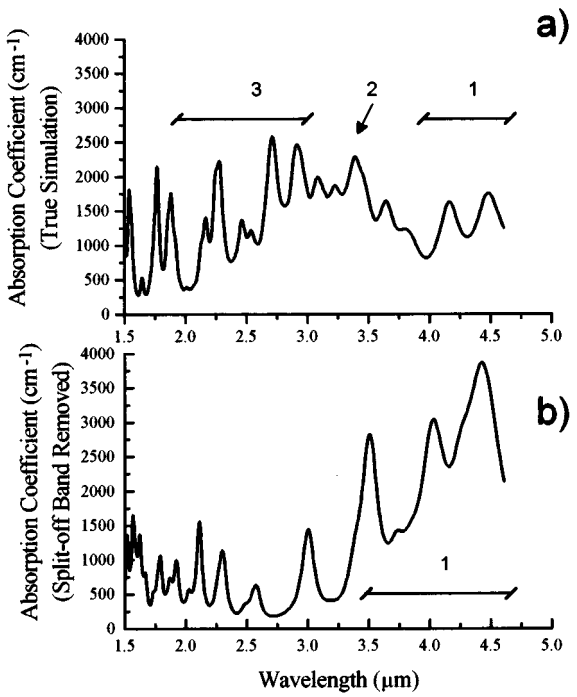

FIG. 9. The calculated absorption coefficient for the $GaAs/Ga_{0.51}In_{0.49}P$ QWIP with the 25-Å-wide well. (a) The true simulation. The number 1 indicates the range of light-hole extended-state absorption. The number 2 points to the split-off bound states. The number 3 indicates the range of split-off extended-state absorption. (b) The second simulation removing the split-off band. The number 1 indicates the significant light-hole extended-state absorption at long wavelengths.

results from the dual influence of split-off extended-state absorption (below 3.4 μm) and light-hole extended-state absorption (above 3.4 μm). It is interesting to note that the ratio of the peak light-hole extended-state absorption to the peak split-off extended-state absorption, as calculated in the true simulation, is very close to the observed intensity ratio of the long- and short-wavelength peak magnitudes in the photoresponse measurement.

V. QUATERNARY SUPERLATTICES

In order to extend the cutoff wavelength of the $Ga_{1-x}In_xAs_yP_{1-y}$ QWIP's to wavelengths in the 8–12-μm atmospheric window, it is necessary to lower the barrier height. Since GaAs and $Ga_{0.51}In_{0.49}P$ represent, respectively, the low and high band-gap energy extremes of the quaternary material system, the extension of the cutoff wavelength can be accomplished in two ways—either through the introduction of quaternary material into the barrier, thereby reducing the band gap of the barrier, or through the introduction of quaternary material into the well, thereby increasing the band gap of the well.

It is important to determine the relative merits of these two approaches. Of particular importance is the influence of the split-off band. Figure 10 shows both the band-gap and split-off energy of quaternary material lattice matched to GaAs as a function of composition from GaAs (0.0) to $Ga_{0.51}In_{0.49}P$ (1.0). Clearly, as compositions move closer to GaAs, the split-off energy increases. Another important factor is the band-offset ratio, which was set to 0.3 for the $GaAs/Ga_{0.51}In_{0.49}P$ QWIP's to fit the theoretical cutoff wavelengths to experiment. It is necessary to determine if this ratio remains constant throughout the $Ga_{1-x}In_xAs_yP_{1-y}$ material system.

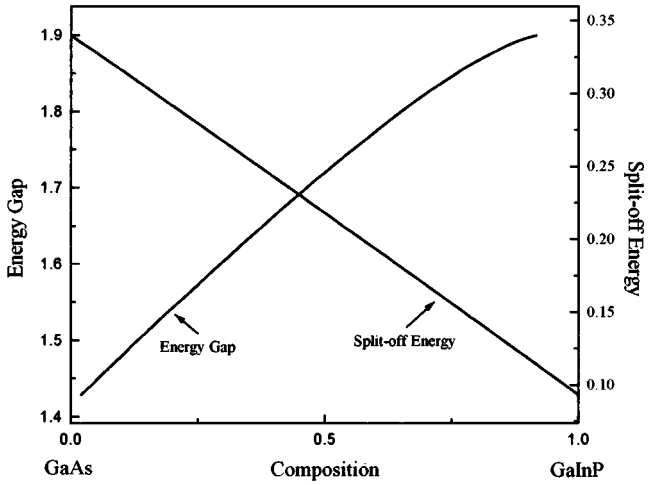

FIG. 10. The room-temperature band gap and split-off energy as a function of composition lattice matched to GaAs.

A quaternary QWIP series was grown to answer these questions. First, a $GaAs/Ga_{0.62}In_{0.38}As_{0.22}P_{0.78}$ QWIP was grown, which reduced the band gap of the barrier material by approximately 100 meV from that of $Ga_{0.51}In_{0.49}P$ (sample A). Second, a $Ga_{0.79}In_{0.21}As_{0.59}P_{0.41}/Ga_{0.51}In_{0.49}P$ QWIP was grown, which increased the band gap of the well material by approximately 100 meV over that of GaAs (sample B). Finally, a $Ga_{0.79}In_{0.21}As_{0.59}P_{0.41}/Ga_{0.62}In_{0.38}As_{0.22}P_{0.78}$ QWIP was grown to extend the cutoff wavelength to approximately 10 μm (sample C).

All three devices were grown by low-pressure metal-organic chemical-vapor deposition with 50 periods of 30-Å-wide wells and 300-Å-wide barriers. The superlattices were sandwiched between top and bottom contacts of GaAs with thicknesses of 0.5 and 1.0 μm, respectively. The doping concentrations in the wells and in the contacts were kept at approximately 3×10^{18} cm^{-3}.

The normalized photoresponse of the three quaternary QWIP's is shown in Fig. 11. The cutoff wavelengths of samples A and B are virtually identical, at approximately 6.5 μm. This is important because it implies that the band-offset ratio is a constant and not dependent on material composition within the $Ga_{1-x}In_xAs_yP_{1-y}$ material system. For a conduction-band offset ratio of 0.3, reducing the band gap of the barrier by 100 meV will reduce the barrier height of the standard quantum well by 70 meV. Similarly, increasing the band gap of the well material by 100 meV will reduce the barrier height of the standard quantum well by 70 meV. If, however, the band-gap offset ratio had not been a constant, then reducing the band gap of the barrier or increasing the band gap of the well would have had no predictable consequence on the cutoff wavelength of the QWIP.

Despite the similarity in cutoff wavelength, the spectral shapes of these two QWIP's are otherwise different. The photoresponse of the $GaAs/Ga_{0.62}In_{0.38}As_{0.22}P_{0.78}$ QWIP rises sharply to a peak around 4.5 μm. It then begins to drop off as expected for a typical p-type QWIP photodetector. However,

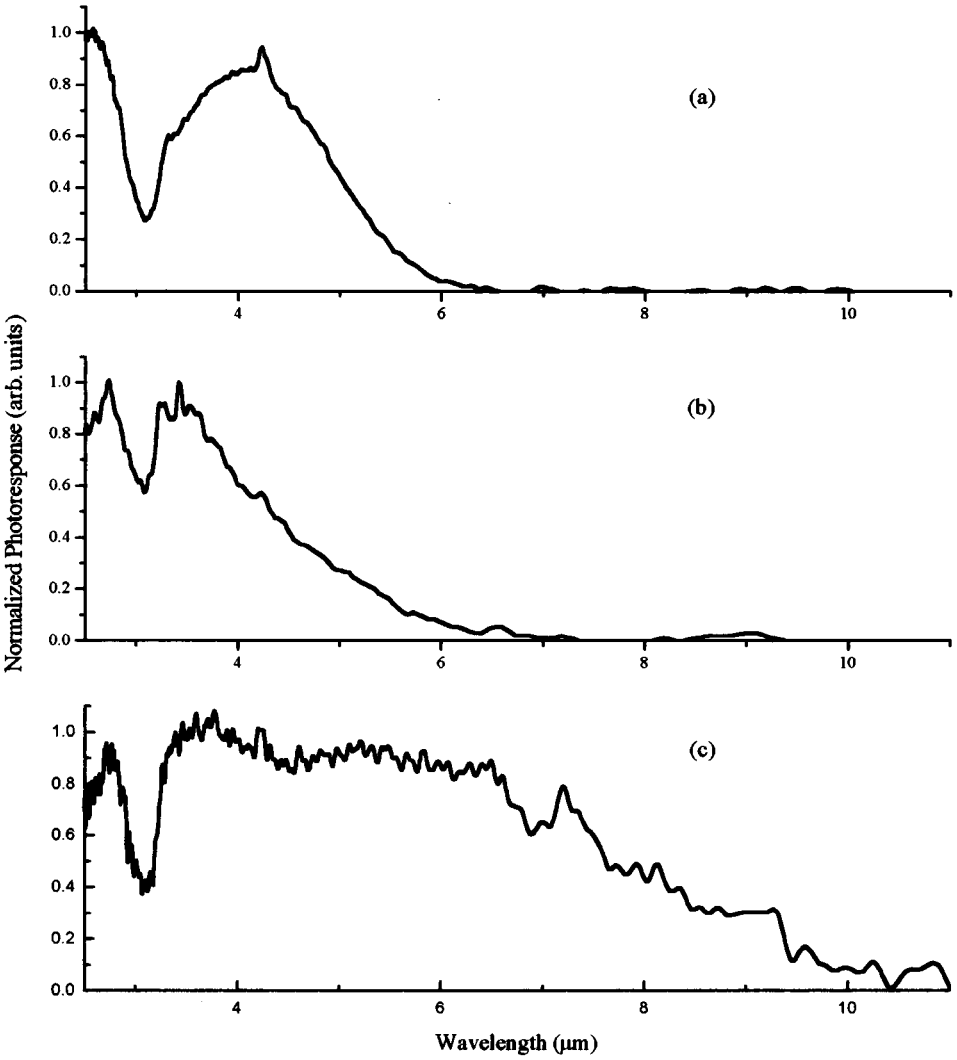

FIG. 11. The photoresponses of the three quaternary QWIP's. (a) The GaAs/ $Ga_{0.62}In_{0.38}As_{0.22}P_{0.78}$ QWIP. (b) The $Ga_{0.79}In_{0.21}As_{0.59}P_{0.41}$/ $Ga_{0.51}In_{0.49}P$ QWIP. (c) The $Ga_{0.79}In_{0.21}As_{0.59}P_{0.41}$/ $Ga_{0.62}In_{0.38}As_{0.22}P_{0.78}$ QWIP.

somewhere between 3 and 4 μm it rises again peaking around 2.5 μm. Unfortunately, the exact position of the onset of this second rise is obscured by water absorption present in our Fourier-transform spectrometer. The photoresponse of the $Ga_{0.79}In_{0.21}As_{0.59}P_{0.41}/Ga_{0.51}In_{0.49}P$ QWIP, on the other hand, has a much more gradual rise peaking between 3 and 3.5 μm, displaying no unexpected features.

The differences between the photoresponse spectra of samples A and B is similar to the differences between the 25-Å GaAs/$Ga_{0.51}In_{0.49}P$ QWIP and the 55-Å GaAs/$Ga_{0.51}In_{0.49}P$ QWIP. Reducing the band gap of the barrier material in sample A has two effects. First, from Fig. 10, it increases the spin splitting energy of the barrier. Second, it allows the second light-hole state to sit in the continuum between the top of the standard quantum well and the bottom of the split-off quantum well. In sample B, the presence of the split-off quantum well at the top of the standard quantum well pushes the second light-hole state into the standard quantum well, making it a bound state. Figure 12 shows the calculated absorption coefficients for each of the three devices.

The long-wavelength absorption of sample A is able to contribute to photoresponse without tunneling, and the fact that the second light-hole state is in the continuum makes the optical absorption strong. The long-wavelength response of sample B results from a combinations of two possible optical transitions. One transition involves the third light-hole state, which has a smaller coupling strength to the heavy-hole ground state than an unbound second light-hole state does. The other transition involves bound states in the spin split-off quantum well, which have a stronger optical coupling than the equivalent transition to an extended state. This factor, combined with the weak coupling to the light-hole extended state, results in a photoresponse that is again dominated by the split-off extended states.

The final QWIP grown in this series was a fully quaternary $Ga_{0.79}In_{0.21}As_{0.59}P_{0.41}/Ga_{0.62}In_{0.38}As_{0.22}P_{0.78}$ QWIP. Figure 13 shows a schematic band diagram of the quantum wells in this device. As the figure indicates, there are two possible absorption mechanisms in this QWIP—bound to light-hole extended-state transitions at lower energies (longer wavelength), and bound to split-off extended-state transitions at higher energies. Figure 11(c) shows the actual photoresponse of this device, which shows significant photoresponse

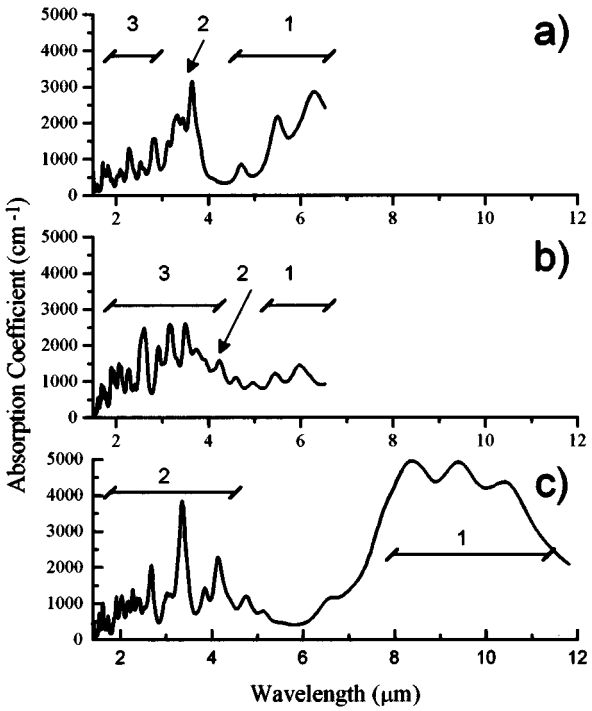

FIG. 12. The calculated absorption coefficient for quaternary QWIP's with 30-Å-wide wells all done with true simulations. (a) The GaAs/$Ga_{0.62}In_{0.38}As_{0.22}P_{0.78}$ QWIP. The number 1 indicates the range of light-hole extended-state absorption made significant by the presence of the second light-hole state in the continuum. The number 2 points to the split-off bound states. The number 3 indicates the range of split-off extended-state absorption. (b) The $Ga_{0.79}In_{0.21}As_{0.59}P_{0.41}/Ga_{0.51}In_{0.49}P$ QWIP. The number 1 indicates the range of light-hole extended-state absorption made insignificant by the binding of the second light-hole state in the standard quantum well. The number 2 points to the split-off bound states. The number 3 indicates the range of the split-off extended state. (c) The $Ga_{0.79}In_{0.21}As_{0.59}P_{0.41}/Ga_{0.62}In_{0.38}As_{0.22}P_{0.78}$ QWIP. The number 1 indicates the range of the light-hole extended state. The number 2 indicates the range of the split-off extended state.

from 2.5 to 10 μm. Note first that just below 5 μm, there is an increase in absorption which peaks around 3.5 μm and then begins to drop off. This is the split-off extended-state absorption. All photoresponse at wavelengths longer than 5 μm is due to the light-hole dominant absorption above the standard barrier. The reason that there is little separation between these two absorption regions is because the well is too narrow pushing the resonant state to higher negative energies far below the top of the standard quantum well. Liu demonstrated that the resonant state in n-type quantum wells needs to be very close to the top of the barrier or the spectral response broadens, and the peak shifts to shorter wavelength.[17] The same holds true for p-type QWIP's.[11] Figure 12(c) shows the calculated absorption coefficient for this device. Note that the peak long-wavelength absorption occurs around 8 μm for the simulation, placing the resonant state approximately 50 meV below the top of the barrier. This high-energy resonant state broadens the spectral response of the light-hole-dominated absorption at long wavelength.

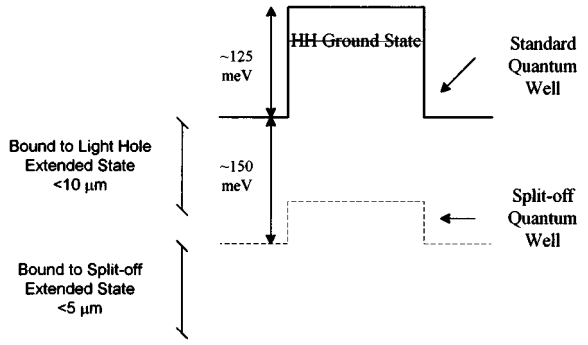

FIG. 13. A graphical depiction of the standard quantum well (formed by the bulk light- and heavy-hole bands) and the split-off quantum well (formed by the bulk split-off bands) for the $Ga_{0.79}In_{0.21}As_{0.59}P_{0.41}/Ga_{0.62}In_{0.38}As_{0.22}P_{0.78}$ QWIP. Due to the narrow well width and the small barrier height of the split-off quantum well, this device exploits both the split-off extended-state and light-hole extended-state absorption, making it photorespond over the range of 2–10 μm.

VI. CONCLUSION

A detailed theoretical analysis compared with the binary-ternary, binary-quaternary, quaternary-ternary, and quaternary-quaternary $Ga_{1-x}In_xAs_yP_{1-y}$ QWIP's grown in our lab has revealed the strong influence of the split-off band on these aluminum-free QWIP's. These devices are capable of a very broad range of spectral response depending on the choice of well and barrier material. Moreover, the choice of well and barrier material also influences the location of the split-off quantum well. By keeping a GaAs well and choosing a quaternary barrier, it is possible to reduce the influence of the split-off band, since the splitting energy of the barrier region increases as the compound moves closer to GaAs. Thus, by using GaAs/$Ga_{1-x}In_xAs_yP_{1-y}$ quantum-well materials, the result would be long-wavelength infrared photodetection based on absorption dominated by bound-to-light-hole extended-state transitions, similar to p-type GaAs/$Al_{0.3}Ga_{0.7}As$ QWIP's. However, it is also possible to keep a ternary barrier and choose a quaternary well which would achieve long-wavelength photodetection based on absorption dominated by bound to split-off extended-state transitions. Finally, broad spectral response is possible through the simultaneous exploitation of both absorption mechanisms.

ACKNOWLEDGMENTS

The work at Northwestern University was supported by Air Force Contract No. F33615-93-C5382 through the Kopin Corporation. The authors would also like to acknowledge Dr. Gerald L. Witt from the U.S. Air Force Office of Scientific Research (AFOSR) for his encouragement, and Dr. Murzy Jhabvala of NASA's Goddard Space Flight Center for his enthusiastic support of this project. The authors would also like to acknowledge the efforts of Christopher Jelen, Steven Slivken, Seongsin Kim, Matthew Erdtmann, and E. Bigan for their work on the growth of these devices. Finally, the authors would like to thank Dr. Frank Szmulowicz for helpful conversations.

[1] B. F. Levine, J. Appl. Phys. **50**, R1 (1993).
[2] Y. Chang and R. B. James, Phys. Rev. B **39**, 12 672 (1989).
[3] S. R. Andrews and B. A. Miller, J. Appl. Phys. **70**, 993 (1991).
[4] J. Hoff, X. He, M. Erdtmann, E. Bigan, and M. Razeghi, J. Appl. Phys. **78**, 2126 (1995).
[5] J. Hoff, S. Kim, M. Erdtmann, R. Williams, J. Piotrowski, E. Bigan, and M. Razeghi, Appl. Phys. Lett. **67**, 22 (1995).
[6] M. Razeghi, *MOCVD Challenge* (Hilger, Bristol, 1989), Vol. 1.
[7] M. Razeghi, *MOCVD Challenge* (Institute of Physics, Bristol, 1995), Vol. 2
[8] M. Razeghi, Nature **369**, 631 (1994).
[9] M. Razeghi, Opt. Photon. News **6** (8), 16 (1994).
[10] F. Szmulowicz, Phys. Rev. B **51**, 1613 (1995).
[11] F. Szmulowicz and G. J. Brown, Phys. Rev. B **51**, 13 203 (1995).
[12] F. Szmulowicz and G. J. Brown, Appl. Phys. Lett. **66**, 1659 (1995).
[13] E. O. Kane, in *Handbook on Semiconductors*, edited by W. Paul (North-Holland, Amsterdam, 1982), Vol. 1, p. 193.
[14] G. A. Baraff and D. Gershoni, Phys. Rev. B **43**, 4011 (1991).
[15] *Semiconductors, Physics of Group IV Elements and III–V Compounds*, edited by K. H. Hellwege and O. Madelung, Landolt-Börnstein, New Series, Group III, Vol. 17, Pt. a (Springer-Verlag, Berlin, 1982).
[16] R. de L. Kronig and W. G. Penney, Proc. R. Soc. London Ser. A **130**, 499 (1930).
[17] H. C. Liu, J. Appl. Phys. **73**, 3062 (1993).